Experimental assessment of the spatial variability of porosity, permeability and sorption isotherms in an ordinary building concrete

N. Issaadi, A. Hamami, Rafik Belarbi, Abdelkarim Aît-Mokhtar

Experimental assessment of the spatial variability of porosity, permeability and sorption isotherms in an ordinary building concrete

N. Issaadi, A.A. Hamami, R. Belarbi*, A. Aït-Mokhtar

University of La Rochelle - CNRS, LaSIE UMR 7356, Avenue Michel Crépeau 17042 La Rochelle Cedex 1, France.

*Corresponding author.
E-mail address: rafik.belarbi@univ-lr.fr, Tel. +33 546 457 239, Fax. +33 546 458 241

Abstract. In this paper, spatial variabilities of some transfer and storage properties of a concrete wall were assessed. The studied parameters deal with water porosity, water vapor permeability (WVP), intrinsic permeability and water vapor sorption isotherms (WVSI). For this purpose, a concrete wall was built in the laboratory and specimens were periodically taken and tested. The obtained results allow highlighting a statistical estimation of the mean value, the standard deviation and the spatial correlation length of the studied fields for each parameter. These results were discussed and a statistical analysis was performed in order to assess for each of these parameters the appropriate probability density function.

Keywords: Concrete, transfer and storage properties, spatial variability, statistical function, correlation length.

1. Introduction

Cementitious materials have a very complex and heterogeneous microstructure leading to random mechanical and physical properties. These properties are affected by different phenomena that may have chemical sources, for instance, cement hydration, or physical sources such as moisture, heat or aggressive species transfers. These latter can vary considerably depending on how the concrete is manufactured, cast and conditioned [1].

Previous works have highlighted the effect of the variability of some concrete parameters on its behavior. De Larrard [2] studied the influence of this variability on concrete leaching and its service life when it is used for manufacturing tunnels for radioactive waste storage. On the other hand, parametric studies of the coupled heat, air and moisture transfer models [3-6] show that the most influencing input parameter is the moisture diffusion coefficient. This was confirmed by Defraeye *et al.* [7]. They showed that the spread of the input parameters uncertainty is related to the dominant mode of moisture migration in the material, which depends on the state of water (liquid or vapor). Trabelsi *et al.* [8, 9] studied the statistical variability of water vapor desorption isotherms and their effect on drying simulations. They showed the impact of this variability on the drying kinetics of concrete, especially for the concrete cover. Dominguez-Minoz *et al.* [10] studied the thermal conductivity of foams and noticed an important variability of this property. They also compared other results provided by an inter-laboratories study on the hydric properties. They noticed a good reproducibility for some properties (porosity and density) when this reproducibility remains very poor for other properties, such as the sorption isotherms and the resistance to the water vapor. Feng *et al.* [11] studied the repeatability and the reproducibility of hydric properties of various materials. They achieved a good repeatability of their results. Nevertheless, the reproducibility was poor, since significant differences were reported for the transport properties due to different experimental procedures and analyses monitoring conditions, when comparing the results obtained by different laboratories [10, 12-14]. Some studies have been devoted to assessing spatial correlation of investigations on concrete structures [15-18].

The present work focuses on the study of the spatial variability of some transfer and storage properties of concrete, mainly porosity, permeability and water vapor sorption isotherm. In addition to the spatial variability study, the repeatability and reproducibility of the intrinsic permeability measurement were studied. For these purposes, three tests per sample were carried out in order to assess the repeatability and two samples were tested for each cored specimen to assess the reproducibility. This part of the study aims to assess if one must integrate the repeatability and the reproducibility measurements during the assessment of spatial variability of the studied property. Results are aimed to be used in future probabilistic approaches for the prediction of hygrothermal behavior, locating potential disorders due to moisture (e.g. mold growth) and durability prediction of construction materials and structures.

The present study is carried out on a concrete wall cast in laboratory. This wall was cored at different spatial locations. The obtained samples were used for the assessment of the above cited properties. Based on the obtained experimental results, statistical distribution density functions were suggested for each property and a correlation length is identified.

2. Experimental program

2.1. Materials

The used concrete was made with Portland-cement (CEM I 52.5 N) complying with the European Standard EN 197–1, a siliceous alluvial sand (0/4 mm) and crushed diorite gravel (10/14 mm). The mix proportions and the main properties are given in Table 1. The used superplasticizer (SP) is CHRYSO Fluid Optima 206. It is based on a modified polycarboxylate. The studied concrete was chosen and designed in order to obtain a compressive strength around 35 MPa at 28 days. This concrete offers good mechanical performances for a use in usual construction fields. Specimens dedicated to the experimental investigation of the spatial variability were cored at 28 days age and stored in a humid chamber at a relative humidity "RH" of 95% and a temperature of 20 °C before tests.

Table 1. Mix proportions (in kg/m^3) and properties of the studied concrete

Cement CEM I 52.5 N (C)	350
Gravel 10/14	1201
Sand (S) 0/4	762
Water (W)	211.8
W/C (-)	0.6
SP/C (%)	2

The mean value, the standard deviation and the spatial correlation of the water porosity, water vapor permeability, intrinsic permeability and water vapor sorption isotherms were assessed on an experimental concrete wall of 2 m of height, 1.20 m of width and 15 cm of thickness. Samples were cored following six vertical lines (Fig. 1): four lines (A, C, D and F) are dedicated to water vapor permeability tests (diameter= 80 mm, height=10 mm), two lines (B and E) are dedicated to air permeability tests (diameter=65 mm, height=50 mm). Specimens cored following the line "A" were characterized on adsorption and desorption at a temperature of 20°C and finally the water porosity test is performed on all the specimens cored from the wall.

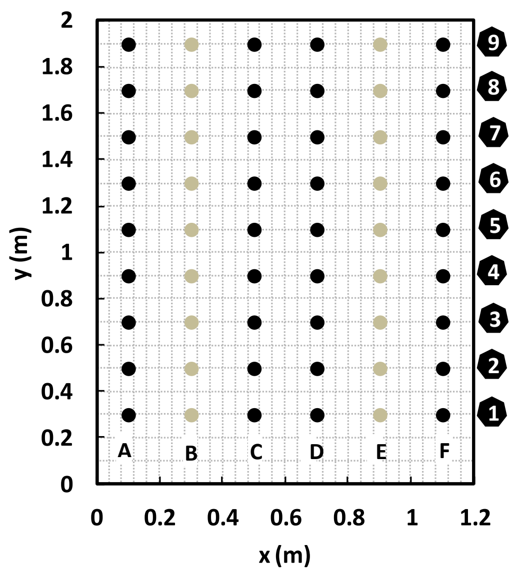

Fig. 1. Cored specimen position in the experimental concrete wall

2.2. Tests and protocols

2.2.1. Preliminary tests

28 days compressive strengths, hydration degree (using thermogravimetric analysis, TGA) and mercury intrusion porosity (MIP) were measured for the assessment of the class of the manufactured concrete and some of microstructural properties.

- Compressive strength

The studied concrete wall was cast in four times with four successive mixes. In each case, compressive strength at 28 days was measured on cylindrical specimens (11x22 cm^3) according to the European standard NF EN 12390-3. These specimens were stored after demolding at 24 hours in a humid chamber at a RH of 95% and a temperature of 20 °C. Compressive strengths obtained on two specimens (Fig. 2) highlight a good homogeneity for each batch, what confirms a good preparation of the various mixtures by following the same mixing procedures.

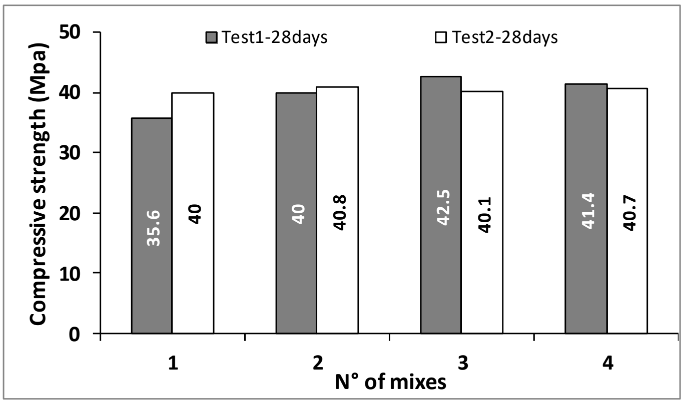

Fig. 2. Compressive strengths of the studied concrete

- Thermogravimetric analysis (TGA)

The experimental investigation of the spatial variability has started after 28 days of concrete age at a quasi-complete hydration, as confirmed by the TGA (Fig. 3) performed as described in [19] on samples at 28 days age. For TGA tests, samples were ground finely (size < 80μm) in order to obtain a homogeneous powder (about 90–100 mg). This powder was kept in a sealed container before being analyzed by TGA 24 h after grinding. TGA tests were carried out under a controlled argon atmosphere with a temperature range of 25–1200 °C and a heating rate of 10 °C/min. Fig. 3 shows the obtained TGA curves. It can be divided on three main phases of the material decomposition according to temperature range. From ambient temperature to 145°C, the curve gives the loss of the free water. From 145 to 600°C, the mass loss relative to the bounded water is given and, from 600 to 800°C the loss corresponds to the decarbonation of the material. Beyond 800°C, no mass loss is observed, this mean that the remaining material does not decompose at this temperature range. Similar results can be found in the literature on cement based materials [20-22].

The corresponding hydration degree calculated according to the relationship of eq. 1 is given in Fig. 3. This parameter is obtained by calculating the ratio between the mass of the bounded water (m_{el}) at the age "t" of the material and the mass of the water required to complete the cement hydration (W_{el}).

$$\alpha(t) = \frac{m_{el}(t)}{W_{el}(\infty).m_c} \tag{1}$$

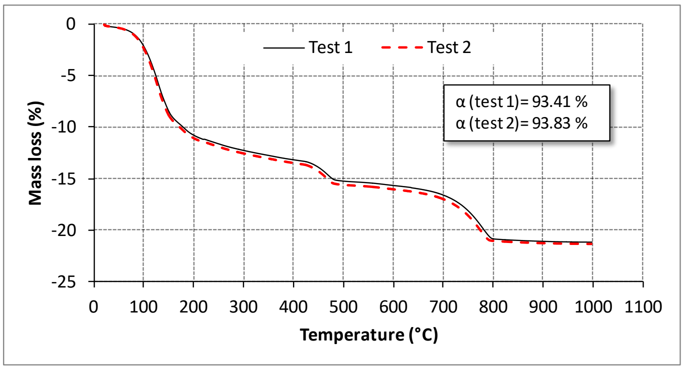

Fig. 3. TGA cumulative curves of concrete at 28 days age

Where $W_{el}(\infty)$ [%] is the mass proportion of the water required to complete the cement hydration. It is estimated at 24% using the cement composition according to the Bogue formula [23]. m_{el} [kg] is the chemically bounded water mass; m_c [kg] is the initial anhydrous cement mass. It is obtained from the initial mass of the tested material and all the compounds of the sample (W/C, S/C, SP/C …). The temperature determining the boundary between the release of free evaporable water and chemically bounded water is fixed at 145 °C according to Mounanga [24]. However, note that literature evokes the destruction of ettringite beyond 60-70°C [25-30]. Therefore, if the temperature threshold is lower, the hydration degree will be higher.

Fig. 3 shows that the average hydration degree is about 93.62%. The obtained hydration degree shows an optimal and almost complete hydration of the used concrete. Consequently, all the possible variability that can be observed would be independent from the hydration process.

- Mercury Intrusion porosimetry

The mercury intrusion porosimetry was carried out on 1 cm^3 concrete sample. The device used is an Autopore form Micromiretics, which can reach injection pressure more than 400 MPa. The obtained concrete pore size distribution is illustrated in Fig. 4 and the mercury porosity value is 14.86 %.

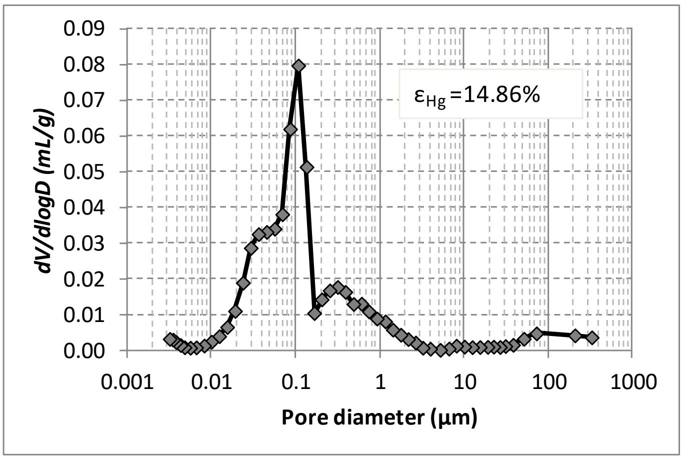

Fig. 4. Pore size distribution of the studied concrete

2.2.2. Transfer parameters studied in the spatial variability framework

Water porosity was performed on 54 cored specimens, water vapor permeability on four vertical lines (lines A, C, D and F: 36 specimens), air permeability on two vertical lines (lines B and E: 36 specimens) and water vapor sorption isotherms on the line A (9 specimens).

- Water porosity

Measurements were performed according to AFPC-AFREM recommendations [31] on cylindrical specimens (5 cm diameter, 2 cm height), sawn from the entire cored specimen from the concrete wall. The porosity Φ can be determined as follows (Eq. 2).

$$\Phi = \frac{M_{air} - M_{oven}}{M_{air} - M_{water}} \times 100\ (\%) \tag{2}$$

Where, M_{air} [kg] and M_{water} [kg] are the weight mass of the saturated sample weighed in air and in water respectively. M_{oven} [kg] is the dry mass of the tested sample.

- Water vapor permeability (WVP)

The measurement of the WVP is performed using the cup method based on the EN ISO 12572 standard [32] in the steady-state regime by using the Gravitest® facility. Samples are discs with 8 cm of diameter and 1 cm of thickness. The test consists on creating a partial vapor pressure gradient between the two compartments at the upstream and the downstream of the sample. This gradient is ensured by two different RH (93% inside the cup and 50% outside) at uniform temperature of 23 °C. The 93 % RH inside the cup is ensured by a saturated salt-water solution of $KN0_3$. At the beginning of the test, the moisture content in the sample is uniform because of the prior pre-conditioning at a temperature of 20 °C and 50% RH suggested by the EN ISO 12572 standard. The test duration is about 20 days, depending on the material diffusivity.

- Intrinsic permeability

First, air permeability measurements were performed using a fully automatic device composed by a “Thermicar® permeameter” and a data acquisition interface in a transitory regime.

To ensure a radial tightness of the samples and a one-directional flow, the latter were laterally surrounded by a resin ring. The measurement procedure is described in Hamami *et al*. [33]. The sample is placed between two pressure chambers. A high pressure P_H is applied in the upstream chamber and kept constant (equal to one of the values: 130 – 160 – 190 – 210 and 350 kPa), whereas a low pressure P_L, initially equal to 8.5 kPa, is applied in the downstream chamber. This low pressure increases according to the air flow through the sample. For each high pressure applied, an apparent permeability “K_A” is obtained according to a modified Darcy’s law (eq. 3).

Secondly, the intrinsic permeability “K_{INT}” is then calculated according to Klinkenberg approach (eq. 4) [34], which is based on the evolution of the apparent permeability “K_A” as a function of the inverse of mean pressure P_m (Eq. 5).

$$K_A = \frac{2\mu L}{P_H^2 - P_L^2} V_L \frac{dP_L^2}{dt} \tag{3}$$

μ [Pa.s] is the air dynamic viscosity, V_L [m^3] is the volume of the downstream chamber and L [m] is the sample thickness.

$$K_{INT} = \frac{K_A\, P_m}{\beta + P_m} \tag{4}$$

β [Pa] is the Klinkenberg factor, which represents the air slip at the interface of the material pores.

$$\frac{1}{P_m} = \frac{2}{P_H + P_L} \tag{5}$$

As mentioned above, repeatability and reproducibility measurement of the intrinsic permeability were carried out. For these purposes, three tests per sample were performed in order to assess the repeatability and, as previously indicated; two samples were tested for each cored specimen to assess the reproducibility.

- Water vapor sorption isotherm (WVSI)

The sample was dried in an oven at 40 °C for 24 h and then degassed under air vacuum to complete the drying. Then, it was weighed to determine the dry mass and then analyzed on the Belsorp aqua-3® device. The used device method is manometric [19]. Samples analyzed are 40 mm of length, 5 mm of width and 5 mm of thickness. The stabilization time is fixed at t=500 s.

3. Results and discussion

- Water porosity

The average porosity values, its standard deviation, coefficient of variation, maximum and minimum values over the considered line are summarized in Table 2. It shows that the water porosities of the cored samples following the six vertical lines (54 specimens) are fairly close.

The standard deviation of porosity on 54 tested samples is equal to 0.78%, which is very close to the result obtained by Aït-Mokhtar *et al.* (0.75%) [14] on High Performance Concrete dried at 105 °C. The same trend is observed for the coefficient of variation: 5.44 % in our case, 6.49 % in [14]. It was found that the water porosity is ranging between 12.64 % and 16.41%.

Table 2. Water porosity: statistical data versus the considered line

Line	A	B	C	D	E	F	All samples
Average (%)	14.13	14.66	14.35	14.19	14.48	14.24	14.34
Standard deviation (%)	0.78	1.08	0.46	0.68	0.94	0.72	0.78
Coefficient of variation (%)	5.55	7.41	3.23	4.80	6.55	5.09	5.44
Minimum (%)	13.12	12.64	13.55	12.99	12.86	13.21	12.64
Maximum (%)	15.12	16.41	14.89	15.50	16.36	15.52	16.41

- Water vapor permeability (WVP)

The average WVP values, its standard deviation, coefficient of variation, maximum and minimum values are summarized in Table 3. It shows that the concrete WVP are ranging between δ_{pmin}=1.37x10^{-12} kg.m^{-1}.s^{-1}.Pa^{-1} and δ_{pmax}=3.6x10^{-12} kg.m^{-1}.s^{-1}.Pa^{-1} with an average value equal to 2.08x10^{-12} kg.m^{-1}.s^{-1}.Pa^{-1}. This result highlights a high dispersion values along the line A with a high standard deviation of 0.74x10^{-12} kg.m^{-1}.s^{-1}.Pa^{-1}. In contrast, a good homogeneity is recorded along the line C with a standard deviation of 0.27x10^{-12} kg.m^{-1}.s^{-1}.Pa^{-1}, which will lead to a low / high correlation length, respectively.

Table 3. WVP: statistical data versus the considered line

Line	A	C	D	F	All samples
Average (x10^{-12}) [kg. m^{-1}.s^{-1}.Pa^{-1}]	2.45	1.97	1.87	2.09	2.08
Standard deviation (x10^{-12}) [kg. m^{-1}.s^{-1}.Pa^{-1}]	0.74	0.27	0.48	0.45	0.54
Coefficient of variation (%)	20.22	14.00	25.79	21.44	25.94
Minimum (x10^{-12}) [kg. m^{-1}.s^{-1}.Pa^{-1}]	1.60	1.60	1.51	1.37	1.37
Maximum (x10^{-12}) [kg. m^{-1}.s^{-1}.Pa^{-1}]	3.60	2.40	3.02	2.89	3.60

- Intrinsic permeability

The final results of the spatial variability of the evolution of intrinsic permeability according to the sample location on the wall are reported in Table 4. This spatial variability is obtained by considering the repeatability and reproducibility measurements (i.e the values are obtained by averaging over the measurements points, the average value of the repeatability and reproducibility tests).

Table 4. Statistical data of the intrinsic permeability for the two vertical lines B and E

	Average $x10^{-17}[m^2]$	Standard deviation $x10^{-17}[m^2]$	Coefficient of variation [%]	Minimum $x10^{-17}[m^2]$	Maximum $x10^{-17}[m^2]$
Line B	3.95	1.03	26.20	2.39	5.91
Line E	3.40	0.89	26.50	2.38	5.28
Both lines	3.66	0.97	26.7	2.38	5.91

The standard deviation does not exceed $0.67x10^{-17}$ m², highlighting good repeatability. Dealing with the reproducibility, the results presented in Fig. 5 give a comparison between the measured values of the intrinsic permeability for the two tested samples per location. Each value corresponds to the average of the three values measured on the same sample.

Fig. 5 shows (i) a significant variation for the intrinsic permeability measured on two samples from the same location (B2) and (ii) permeability remains constant for the two tested samples (B5). Globally, this means that the intrinsic permeability depends on the spatial location of the sample. The permeability appears to be minimal at the middle of the vertical line and maximal at the top of the wall (Fig. 5).

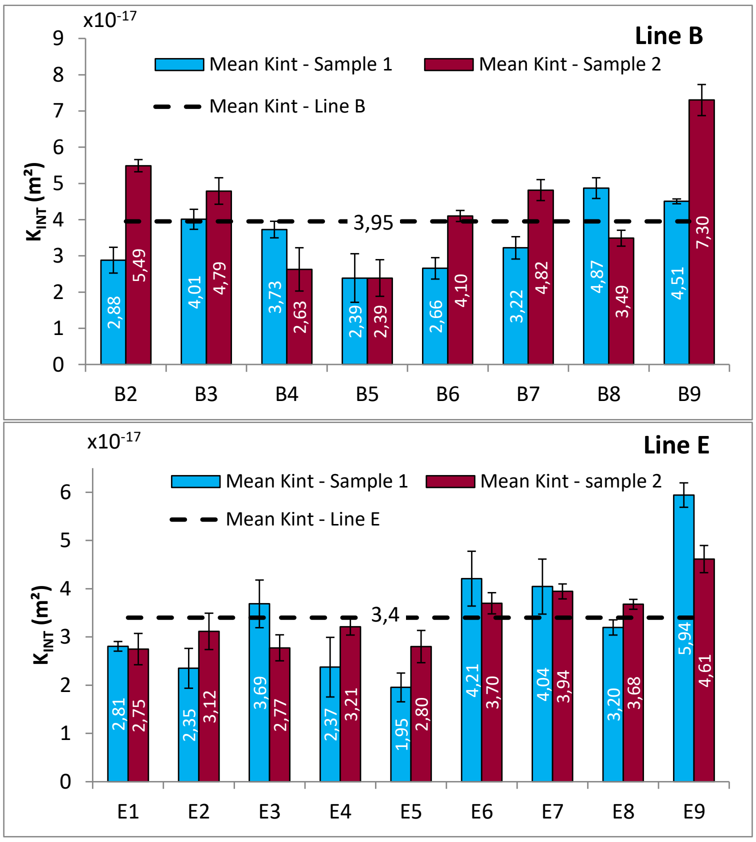

Fig. 5. Reproducibility of intrinsic permeability measurements along the vertical lines B & E

The intrinsic permeability obtained by performing repeatability tests was found between 1.95×10^{-17} and 7.3×10^{-17} m^2 with an average value equal to 3.65×10^{-17} m^2. This result is in good agreement with those obtained by [14, 35]. Note that the variability is reduced when the reproducibility test is carried out (Fig. 5). In this case, intrinsic permeability was found between 2.38×10^{-17} and 5.91×10^{-17} m^2 with an average value of 3.66×10^{-17} m^2. This greatly affects the standard deviation of the studied properties. Consequently, the generated random fields of intrinsic permeability will be modified.

To go further these results, the spatial distribution of water porosity, water vapor permeability and intrinsic permeability are fitted by an appropriate probability density function (Fig. 6). To assess the probability density function that best represents the statistical distribution of the experimental data, an approach by the maximum likelihood estimator was used [36, 37]. Using this method, Table 5 summarizes the average and variance of each proposed function with its corresponding "Log likelihood".

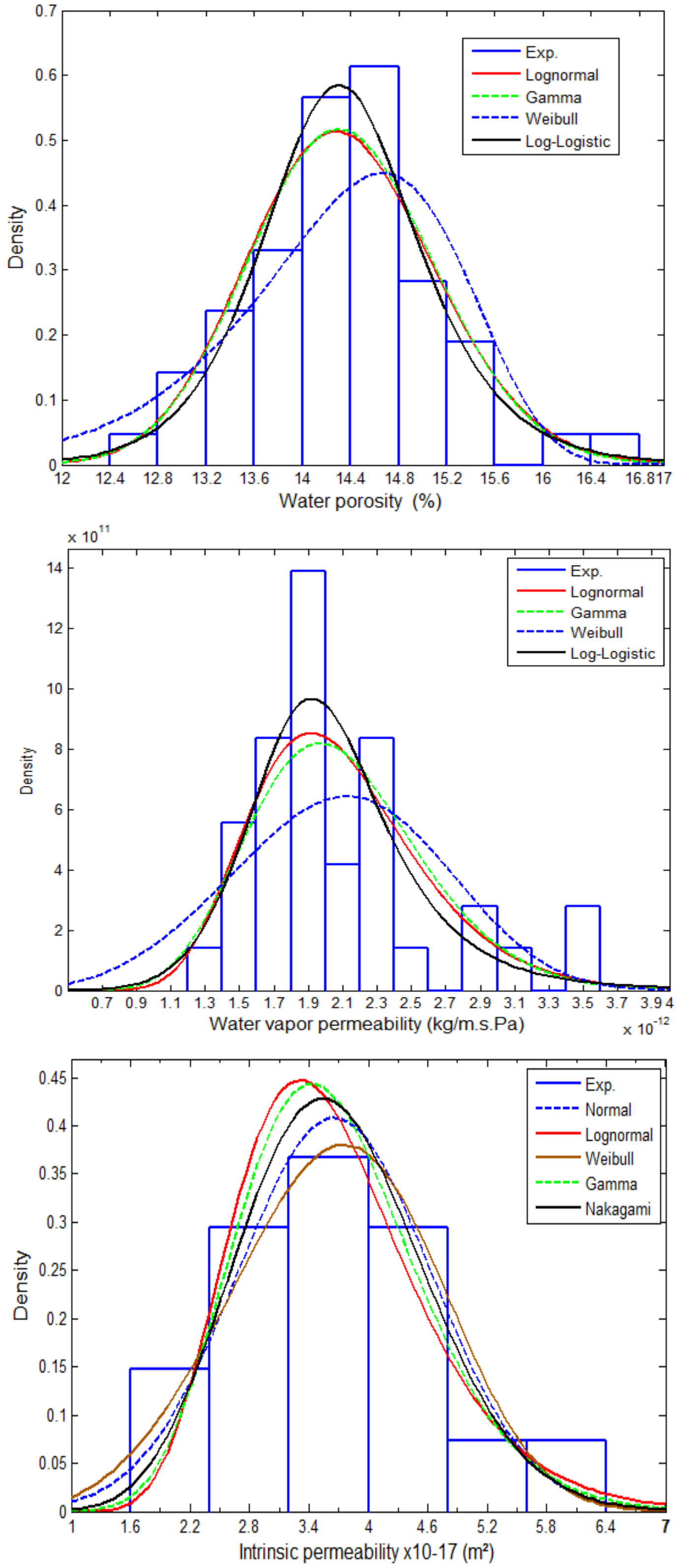

Fig. 6. Distribution of water porosity, water vapor permeability and intrinsic permeability. The lines are the fitted probability densities

For the water porosity, the Log-logistic distribution seems to be the most appropriate to reproduce the experimental values with an expectation $\mu = 14.35$ % and a variance $\sigma^2 = 0.60$ %. This result joins literature ones [14], where Log-normal, Gamma, Birnbaum-Sanders and Log-logistic probability functions are suggested. For the WVP, the Log-normal and Log-logistic density distributions are the most appropriates. In a second position, there is a Gamma and Weibull distribution.

Finally, for the intrinsic permeability, the Log-normal and Weibull density functions seem to be the most appropriate to reproduce the statistical distribution of the combined repeatability and reproducibility measurements. These two functions present approximately the same average (3.65×10^{-17} m²) and a variance of 0.95×10^{-34} m^4 and 1.04×10^{-34} m^4, respectively. As mentioned in the literature [14], from a practical point of view and in the perspective of using these results in future probabilistic approaches for the prediction of hygrothermal behavior and materials durability, it may be wise to use “classical” probability functions with parameters that are easy to estimate, rather than functions that are more difficult to use in simulations (e.g. random fields). From this point of view, the log-normal distribution seems to be one of the most appropriate distributions [14].

Table 5. Water porosity, water vapor permeability and intrinsic permeability: parameters of the tested probability density function

Property	Distribution density function	Log-normal	Gamma	Weibull	Log-logistic	
Water porosity	Average (%)	14.34	14.34	14.28	14.34	
	Variance	0.61	0.59	0.96	0.60	
	Log likelihood	-61.39	-61.43	-66.87	-61.06	
Water vapor permeability	Average (x10^{-12})	2.08	2.08	2.07	2.04	
	Variance (x10^{-25})	2.52	2.49	3.60	2.59	
	Log likelihood	970.46	969.34	964.67	970.30	
Distribution density function		Normal	Log-normal	Weibull	Gamma	Nakagami
Intrinsic permeability	Average x10^{-17}	3.65	3.66	3.65	3.65	3.66
	Variance x10^{-34}	0.95	0.94	1.04	0.85	0.86
	Log likelihood	-23.23	-22.26	-23.60	-22.43	-22.72

- Water vapor sorption isotherm

Fig. 7 illustrates the variability of the WVSI at 20 °C of the samples taken along the line A of the concrete wall. The variability increases in adsorption and desorption, according to the range of the considered RH. Two envelope curves are observed. They concern that of the sample A1 (lower curve) and that of A9 (upper curve). This can be justified by the values of the water porosity of these samples (Φ_{A1}=13.3% and Φ_{A9}=15%), while those of the other samples are located inside these limits. In addition, water content disparities of about 1.60 % in adsorption and 3.10 % in desorption are registered in the vicinity of 95 % of RH.

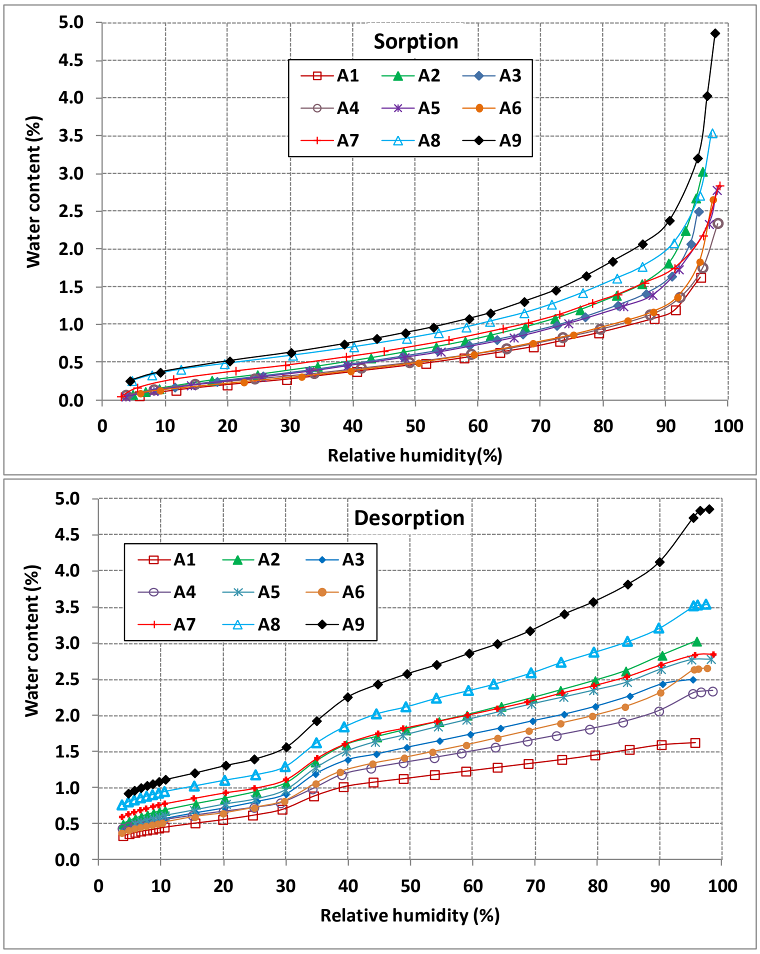

Fig. 7. WVSI variability of the samples taken according to the line A

Fig. 8 shows the mass water content dispersion in adsorption and desorption processes at RH(%)≈{5; 30; 50; 70 and 95} according to the sample position in the wall. Table 6 gives the average water content values measured at equilibrium according to the cited range of RH, the corresponding standard deviations and coefficients of variation. These results confirm:

- (i) the high dispersion at the higher RH. Indeed, the standard deviation determined at 5% of RH is approximately equal to 0.09%; it is lower than standard deviation obtained at 95% of RH (0.56%) (Table 6);

- (ii) it shows a higher dispersion in water content in desorption compared to those measured in adsorption. In fact, the standard deviations of water content obtained in desorption are higher than those determined in adsorption (Table 6).

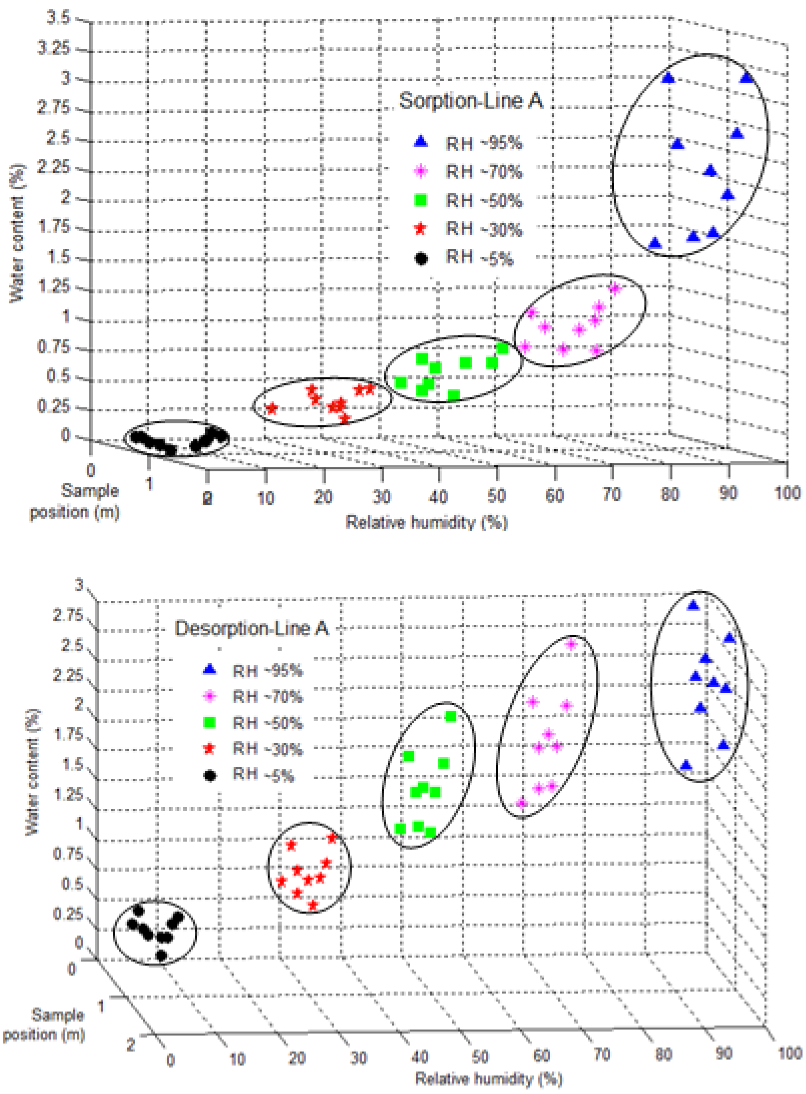

Fig. 8. Water content dispersion at RH (%)≈{5; 30; 50; 70 and 95}

Table 6. WVSI: average value, standard deviation and coefficient of variation of water content in adsorption and desorption according to RH levels

	RH (%)	5	10	30	50	70	95
Adsorption	Average (%)	0.12	0.21	0.43	0.66	1.05	2.35
	Standard deviation (%)	0.09	0.11	0.12	0.17	0.22	0.56
	Coefficient of variation (%)	75.00	53.83	27.90	25.75	20.95	23.83
Desorption	Average (%)	0.56	0.69	1.02	1.72	2.12	2.89
	Standard deviation (%)	0.19	0.22	0.27	0.44	0.54	0.87
	Coefficient of variation (%)	33.92	31.88	26.47	25.58	25.47	30.10

- Correlation length identification

Using probabilistic approaches that take into account spatial variability of the inputs parameters requires assessing the spatial correlation of the studied property fields. This is defined by the correlation length noted “Lc”, which allows estimating the distance between two testing points at which the measured values become independent [15]. It reflects the importance of the spatial correlation of random fields used in the probabilistic approach implementation. The higher the correlation length, the stronger is the correlation of the field. This parameter is identified using a variogram based on the experimental values previously presented. The variogram is a practical mean for describing the spatial correlation of measurements. On one hand, it is a tool to investigate and quantify the spatial variability of the parameter studied. On the other hand, most geostatistical estimation or simulation algorithms require an analytical variogram model, which can be obtained from the experimental variogram [33, 39]. The variogram at the lag distance “d” is expressed as follows (Eq. 6).

$$\gamma(d) = \frac{1}{2|N(d)|}\sum_{(i,j)\,\epsilon\, N(d)}\left|Y_i - Y_j\right|^2 \tag{6}$$

Where

$$N(d) = \left\{(i,j)\backslash\left|\mathrm{x_i} - \mathrm{x_j}\right| = \mathrm{d}\right\} \tag{7}$$

Where $\gamma(d)$ is the variogram value; Y_i is the value of the studied property at the x_i position; N(d) is the set of pairs of points (i, j) such as the distance between these points is equal to d (number of pairs that satisfy this condition).

The relationship between the covariance (C) and the variogram is defined by Eq. 8. Note that the covariance on 0 is the variance. By knowing the variogram value corresponding to each distance, one can deduce from Eq. 8 the value of the covariance. Then, it is enough to optimize the value of the correlation length "Lc" in the covariance functions which can be expressed by Eq. 9 as follows:

$$\gamma(d) = C(0) - C(d) \tag{8}$$

$$C(x, y) = \sigma^2 \exp\left(-\frac{\|x_i - x_j\|^2}{L_c^2}\right) \tag{9}$$

Where C(x,y) is the covariance between the two points x_i and x_j. Each term C_{ij} of the covariance matrix "C" is the value of the covariance function calculated between the nodes i and j. The vectors x_i and x_j give the position of the corresponding nodes.

Fig. 9 shows a comparison between the covariance values measured on the experimental concrete wall and those obtained using the corresponding covariance functions. The normalized covariance relative to the variance is presented on the y-axis. We note that the correlation length value is ranging from 0.36 to 1.88 m for the water porosity, from 0.28 to 0.61 m for the water vapor permeability and from 0.62 to 0.68 m for the intrinsic permeability. Regarding the correlation length of WVSI, identification was undertaken according to the RH levels in adsorption and desorption process (RH≈5 ; 10 ; 30 ; 50 ; 70 and 95 %) of the line A (Fig. 10). The adsorption correlation length reaches its maximum in RH around 5%. In this region the dispersion of water content is very low (Fig. 8). This is not the case in desorption phase. Low correlation lengths are recorded for higher RH. This result means that there are a high dispersion and a low dependency of the spatial water contents in the capillary condensation zone, where the transfer is mainly governed by the liquid transport. In conclusion, the characteristics of the WVSI random fields depend on the considered RH. They are generally highly correlated in the low RH region and less correlated in the vicinity of the saturation zone.

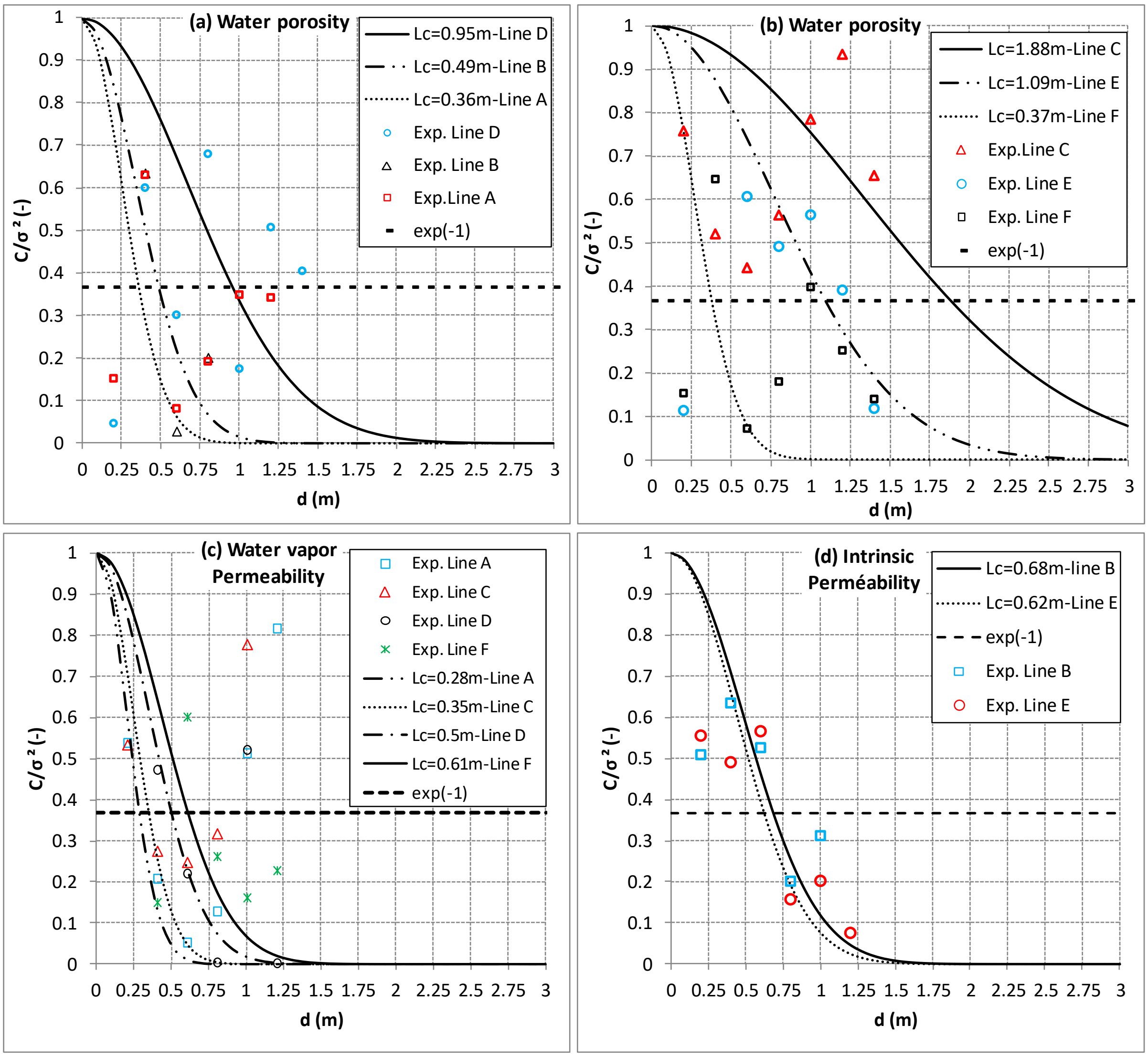

Fig. 9. Identification of the correlation lengths of the water porosity (a & b), WVP (c) and intrinsic permeability (d)

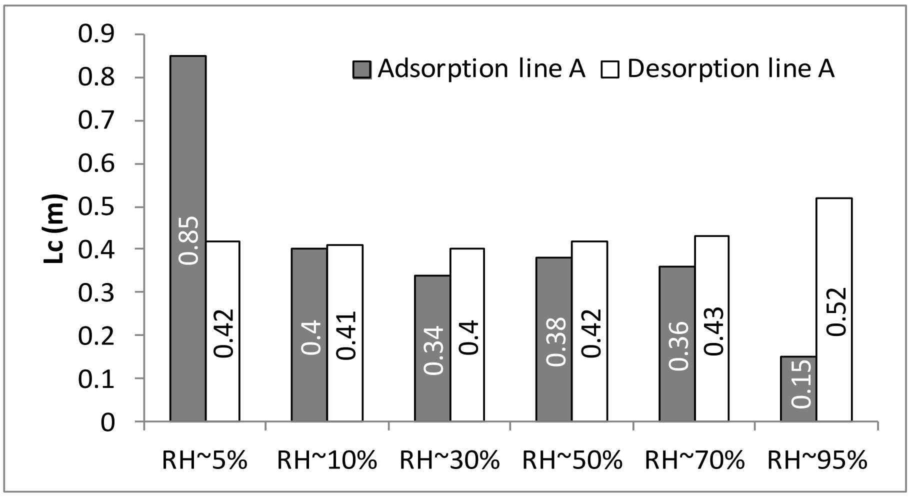

Fig. 10. Correlations lengths histograms in adsorption and desorption according to the line "A" as a function of RH

Impact of spatial variability of water vapor permeability of concrete on their hygrothermal behavior is assessed. This is performed on a concrete wall with initial condition of T_0=20°C and RH_0=50% subjected to a boundary conditions of (T_1=20°C, RH_1=65%) and (T_2=40°C, RH_2=80%) (Fig. 11-a). The study is performed to assess the evolution of the relative humidity at 9 points of the concrete wall located at the same depth (18 cm), as shown in (Fig. 11-b).

The obtained results are presented in Fig. 12. The deterministic simulation is performed by considering an average value of water vapor permeability $\delta_p = 2{,}086\ \times 10^{-12}\ kg/m.s.Pa$. This result highlights the impact of the spatial variability of the water vapor permeability on the relative humidity distribution that can reach 10% of RH. In contrast with deterministic simulation that gives a homogeneous distribution along the wall, taking into account the particular spatial variability of some influential transfer parameters of the studied material shows a difference in their hygrothermal behavior.

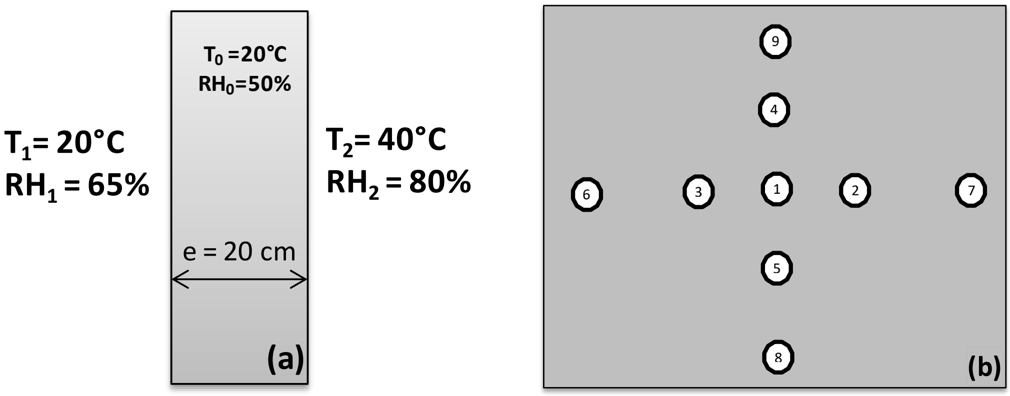

Fig. 11. Boundary conditions (a) and location of the studied points in the wall for the water content assessment (b)

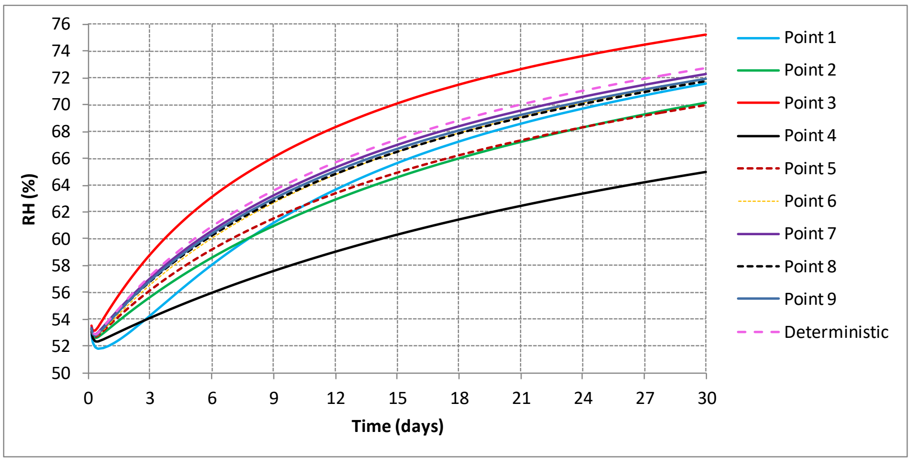

Fig. 12. Relative humidity distribution at the located studied points (point 1 to 9)

This work focuses on highlighting the spatial variability of some transfer properties of concrete, which is widely used in building construction. Our objective is to bring attention to the particular variability of this material, which makes deterministic approaches irrelevant in studies of transport in porous media.

4. Conclusions

Spatial variability of water porosity, water vapor permeability, intrinsic permeability and water vapor sorption isotherms were assessed. These latter are mainly involved in hygrothermal behavior and durability assessment for cement-based materials in building envelops and concrete structures. The coefficient of variation obtained for water porosity is 5.44 % and 26 % for water vapor permeability. Good repeatability and reproducibility of the intrinsic permeability measurements on each tested sample is observed. An increase of the water contents variability in adsorption and desorption, according to the range of the relative humidity is noted. These results constitute a database that can be used as input data for probabilistic approaches. It can be used by considering the fitting probabilistic density functions or as input parameters for generating random fields by using for example Karhunen-Loeve expansion. This would be the subject of a future work. In addition, variability of other transfer parameters of cement-based materials could also be studied using this approach, such as microstructure linked to permeability variability [40-41] or in the determination of chloride diffusion coefficients [42-43] to improve some literature deterministic approaches in studying durability of cementitious structures.

References

[1] Delmi M M Y, Aït-Mokhtar A, Amiri O (2006) Modeling the coupled evolution of hydration and porosity of cement-based materials. Constr Build Mater 20:504-514.

[2] De Larrard T, Benboudjema F, Colliat J B, Torrenti J M (2012) Influence of the spatial variability of leaching kinetics parameters on the lifespan of a concrete structure. Eur J Environ Civ Eng 15:606-624.

[3] Luikov A (1966) Heat and mass transfer in capillary-porous bodies. First Ed. Pergamon press, Oxford.

[4] Qin M, Belarbi R (2005) Development of an analytical method for simultaneous heat and moisture transfer in building materials utilizing transfer function method. J Mater Civ Eng 17: 492-497.

[5] Qin M, Belarbi R, Aït-Mokhtar A, Nilsson L (2007) Simultaneous heat and moisture transport in porous building materials: Evaluation of non-isothermal moisture transport properties. J Mater Sci 43:3655-3663.

[6] Abahri K, Belarbi R, Trabelsi A (2011) Contribution to analytical and numerical study of combined heat and moisture transfers in porous building materials. Build Environ 46:1354-1360.

[7] Defraeye T, Blocken B, Carmeliet J (2013) Influence of uncertainty in heat–moisture transport properties on convective drying of porous materials by numerical modeling. Chem Eng Res Des 91:36-42.

[8] Trabelsi A, Hamami A, Belarbi R, Turcry P, Aït-Mokhtar A (2012) Assessment of the variability of moisture transfer properties of High Performance Concrete from multi-stages drying experiment. Eur J Environ Civ Eng 16:352–361.

[9] Trabelsi A, Belarbi R, Turcry P, Aït-Mokhtar A (2011) Water vapour desorption variability of in-situ concrete and effect on drying simulations. Mag Concr Res 63:333-342.

[10] Dominguez-Munoz F, Anderson B, Cejudo-Lopez J, Carrillo-Andres A (2010) Uncertainty in the thermal conductivity of insulation materials. Energy Build 42:2159-2168.

[11] Feng C, Janssen H, Feng Y, Meng Q (2015) Hygric properties of porous building materials: Analysis of measurement repeatability and reproducibility. Build Environ 85:160-172.

[12] Roels S, Carmeliet J, Hens H, Adan O (2004) Interlaboratory comparison of hygric properties of porous building materials. J Therm Envel Build Sci 27:307-325.

[13] Roels S, Talukdar P, James C, Simonson C J (2010) Reliability of material data measurements for hygroscopic buffering. Int J Heat Mass Transfer 53:5355–5363.

[14] Aït-Mokhtar A, Belarbi R, Benboudjema F et al (2013) Experimental investigation of the variability of concrete durability properties. Cem Concr Res 45:21-36.

[15] De Larrard T, Benboudjema F, Colliat J B, Torrenti J M (2012) Caractérisation expérimentale de la variabilité spatiale des propriétés d'un béton: Identification des longueurs de corrélation et recherche de corrélations entre indicateurs de durabilité. JFMS2012, Chambéry, France.

[16] Schoefs F, Tran T V, Bastidas-Arteaga E, Villain G, Derobert X, O'Connor A, Bonnet S (2012) Optimization of non-destructive testing when assessing stationary stochastic processes: application to water and chloride content in concrete. International Conference Durable Structures (ICDS12), Lisbon – Portugal.

[17] O'Connor A J, Kenshel O (2013) Experimental evaluation of the scale of fluctuation for spatial variability modeling of the chloride-induced reinforced concrete corrosion. J Bridge Eng 18:3-4.

[18] Boéro J, Schoefs F, Yáñez-Godoy H, Capra B (2012) Time-function reliability of harbour infrastructures from stochastic modeling of corrosion. Eur J Environ Civ Eng 16:1187-1201.

[19] Issaadi N, Nouviaire A, Belarbi R, Aït-Mokhtar A (2015) Moisture characterization of cementitious material properties: Assessment of water vapor sorption isotherm and permeability variation with ages. Constr Build Mater 83:237-247.

[20] Taylor H F W, Turner A B (1987) Reactions of tricalcium silicate paste with organic liquids. Cem Concr Res 17: 613–623.

[21] Loukili A, Khelidj A, Richard P (1999) Hydration kinetics, change of relative humidity and autogenous shrinkage of ultra-high-strength concrete. Cem Concr Res, 29: 577-584.

[22] Méthodes de mesure et d'essai de Laboratoire. Méthodes d'essai n°58 : Caractéristiques microstructurales et propriétés relatives à la durabilité des bétons. Techniques et Méthodes des LPC, 2002, p. 17-22.

[23] Bogue R H (1952) La chimie du ciment de Portland, Eyrolles Edition, Paris.

[24] Mounanga P (2003) Étude expérimentale du comportement de pâtes de ciment au très jeune âge : hydratation, retraits, propriétés thermophysiques. (PhD Thesis), University of Nantes, France.

[25] Lawrence C D (1995) Mortar expansions due to delayed ettringite formation : effects of curing period and temperature. Cem Concr Res 25:903–914.

[26] Taylor H F W, Famy C, Scrivener K L (2001) Delayed ettringite formation. Cem Concr Res 31:683–693.

[27] Collepardi M (2003) A state-of-the-art review on delayed ettringite attack on concrete. Cem Concr Compos 25:401–407.

[28] Sahu S, Thaulow N (2004) Delayed ettringite formation in Swedish concrete railroad ties. Cem Concr Res 34:1675-1681.

[29] Escadeillas G, Aubert J E, Segerer M, Prince W (2007) Some factors affecting delayed ettringite formation in heat-cured mortars. Cem Concr Res 37:1445–1452.

[30] Pavoine A, Brunetaud X, Divet L (2012) The impact of cement parameters on Delayed Ettringite Formation. Cem Concr Compos 34 :521–528.

[31] AFPC-AFREM (1997) Méthodes recommandées pour la mesure des grandeurs associées à la durabilité. Compte rendu des journées techniques AFPC-AFREM.

[32] NF EN ISO 12572 (2001) Performance hygrothermique des matériaux et produits pour le bâtiment - Détermination des propriétés de transmission de la vapeur d'eau.

[33] Hamami A A, Turcry P, Aït-Mokhtar A (2012) Influence of mix proportions on microstructure and gas permeability of cement pastes and mortars. Cem Concr Res 42:490-498.

[34] Klinkenberg L J (1941) The permeability of porous media to liquid and gases. Drill Prod Pract Am Pet Inst 200-214.

[35] Gallé C, Sercombe J (2011) Permeability and pore-structure evolution for silico-calcareous and hematite high-strength concretes submitted to high temperatures, J Mat Struct 34:619-628.

[36] Fisher R A (1922) On the mathematical foundations of theoretical statistics. Philos Trans R Soc A 222:309–368.

[37] Edwards A W F (1972) Likelihood, Cambridge University Press, 243 pp.

[38] Nguyen N T, Sbartaï Z M, Lataste J F, Breysse D, Bos F (2013) Assessing the spatial variability of concrete structures using NDT techniques – Laboratory tests and case study. Constr Build Mater 49:240-250.

[39] Gringarten E, Deutsch C V (2001) Variogram interpretation and modeling. Math Geol 33:507-534.

[40] Aït-Mokhtar A, Amiri O, Dumargue P, Sammartino S (2002) A new model to calculate water permeability of cement-based materials from MIP results. Adv Cem Res 14(2): 43-49.

[41] Amiri O, Aït-Mokhtar A, Sarhani M (2005) Tri-dimensional modelling of cementitious materials permeability from polymodal pore size distribution obtained by mercury intrusion porosimetry tests. Adv Cem Res 17(1): 39-45.

[42] Amiri O, Aït-Mokhtar A, Seigneurin A (1997) A complement to the discussion of A. Xu and S. Chandra about the paper "calculation of chloride coefficient diffusion in concrete from ionic migration, measurements" by C. Andrade. Cem Concr Res 27(6): 951-957.

[43] Amiri O, Aït-Mokhtar A, Dumargue P, Touchard G (2001) Electrochemical modelling of chlorides migration in cement based materials. Part II: Experimental study - Calculation of chlorides flux. Electrochim Acta 46(23): 3589-3597.